中性子星クラストとパスタ原子核

飯田　圭（高知大学）

共同研究者：　親松和浩（愛知淑徳大）、渡辺元太郎（APCTP）、佐藤勝彦（NINS）
中里健一郎（東京理科大）、祖谷元（国立天文台）

パスタ原子核の基本性質

中性子星内部にパスタ原子核はあるか？

軟ガンマ線リピーターの巨大フレアとクラスト内部の原子核

Systems composed of nuclear matter

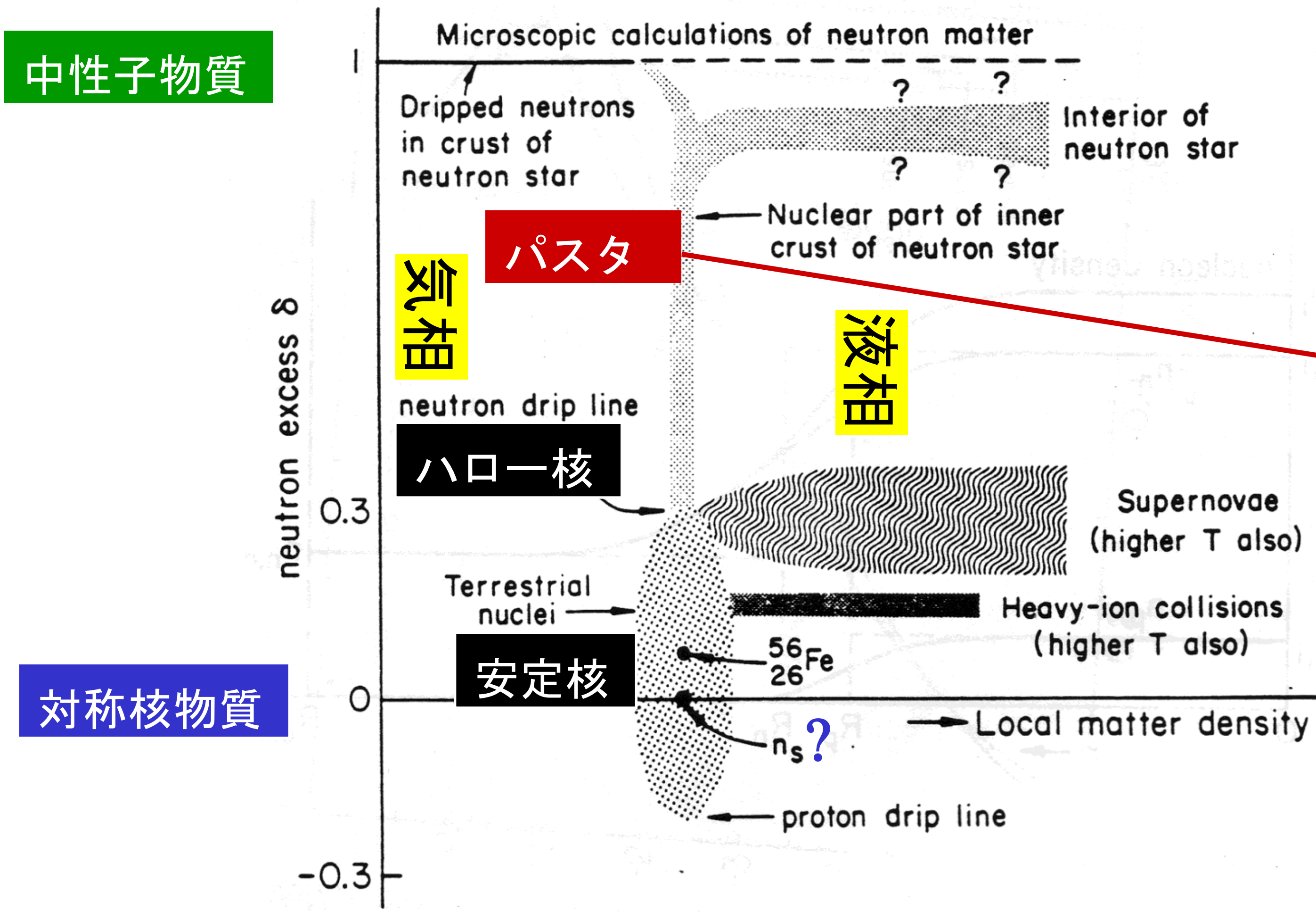

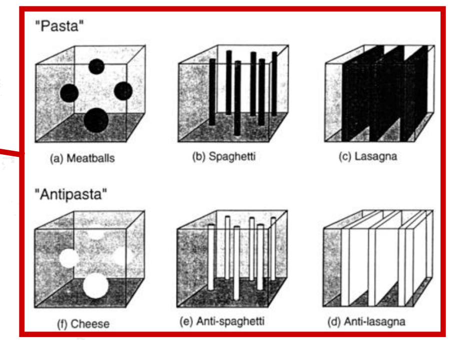

From Lamb (1991).

Pethick & Ravenhall, ARNPS **45** (1995) 429.

Phenomenological EOS parameters

Energy per nucleon of bulk nuclear matter near the saturation point (nucleon density n, neutron excess α):

$$w = w_0 + \frac{K_0}{18n_0^2}(n-n_0)^2 + \left[S_0 + \frac{L}{3n_0}(n-n_0)\right]\alpha^2$$

n_0, w_0	saturation density & energy of symmetric nuclear matter
S_0	symmetry energy coefficient
K_0	incompressibility
L	density symmetry coefficient

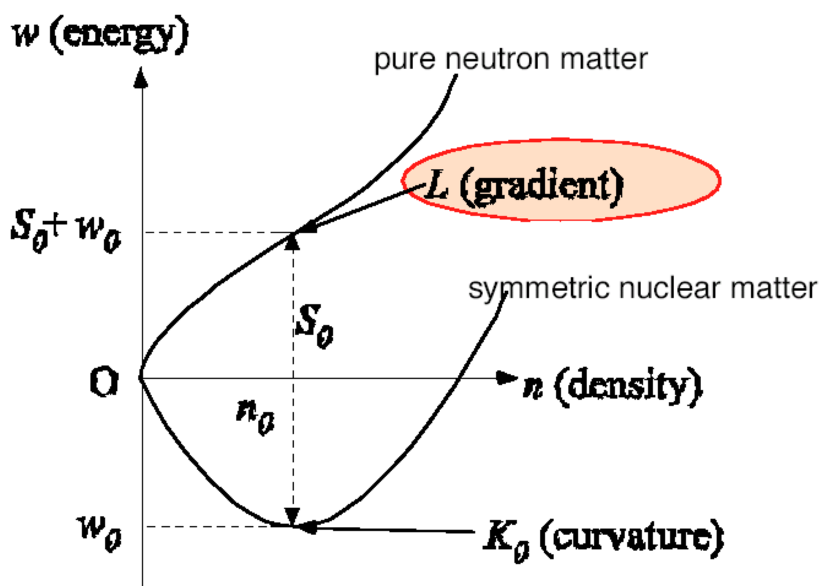

ゼロ温度での核物質の状態方程式

非圧縮率 →

対称エネルギーの密度勾配 ↑

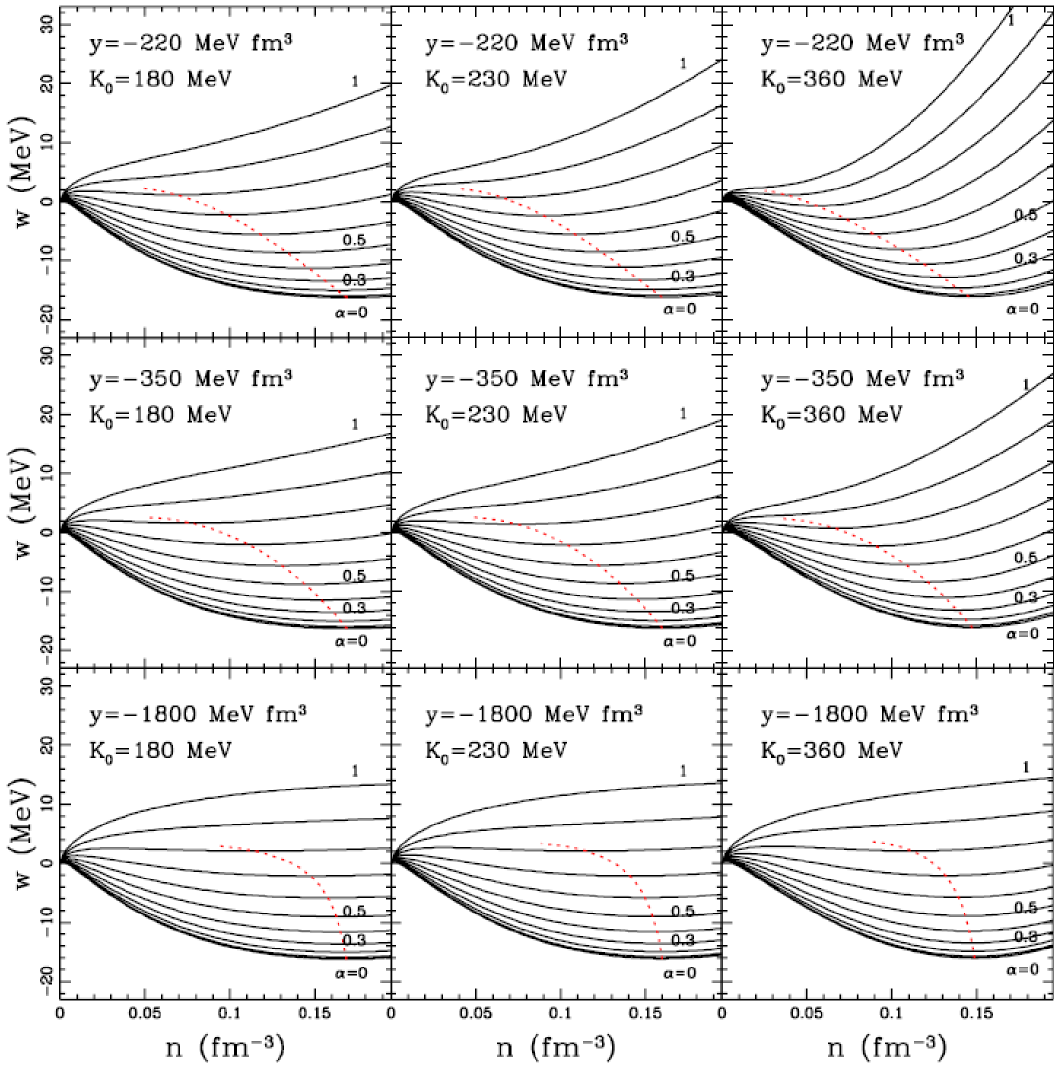

9つの極端な例

・安定核の半径・質量データは同様に再現

・将来の不安定核データで峻別可能？

Ref. Oyamatsu & Iida, PTP **109** (2003) 631 ; Kohama, Iida, & Oyamatsu, PRC **72** (2005) 024602.

中性子星断面の予想図

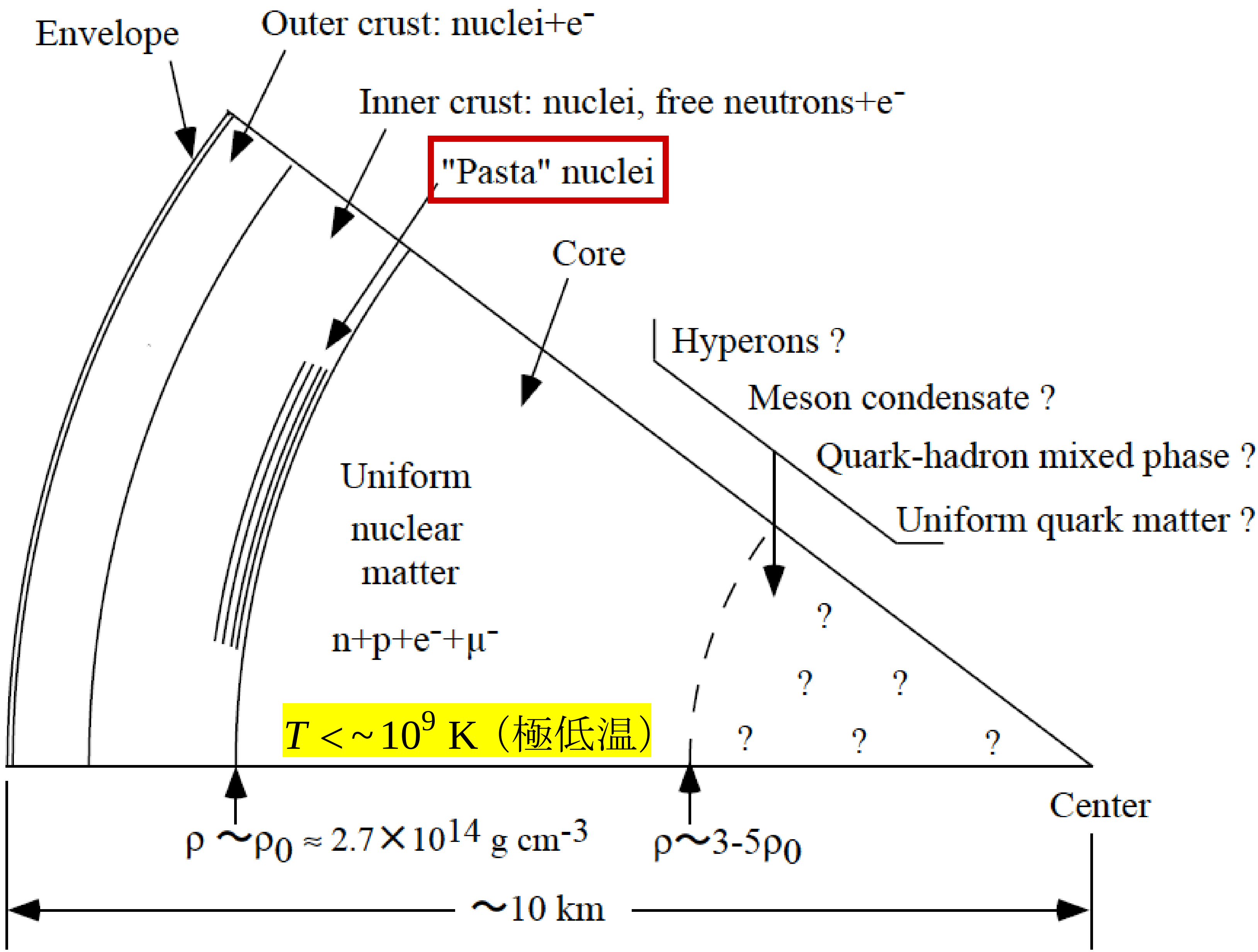

Envelope
Outer crust: nuclei+e⁻
Inner crust: nuclei, free neutrons+e⁻
"Pasta" nuclei
Core
Hyperons ?
Meson condensate ?
Quark-hadron mixed phase ?
Uniform quark matter ?
Uniform nuclear matter
n+p+e⁻+μ⁻
$T <\sim 10^9$ K（極低温）
?
Center
$\rho \sim \rho_0 \approx 2.7 \times 10^{14}$ g cm^{-3}
$\rho \sim 3\text{-}5\rho_0$
～10 km

Nuclear pasta

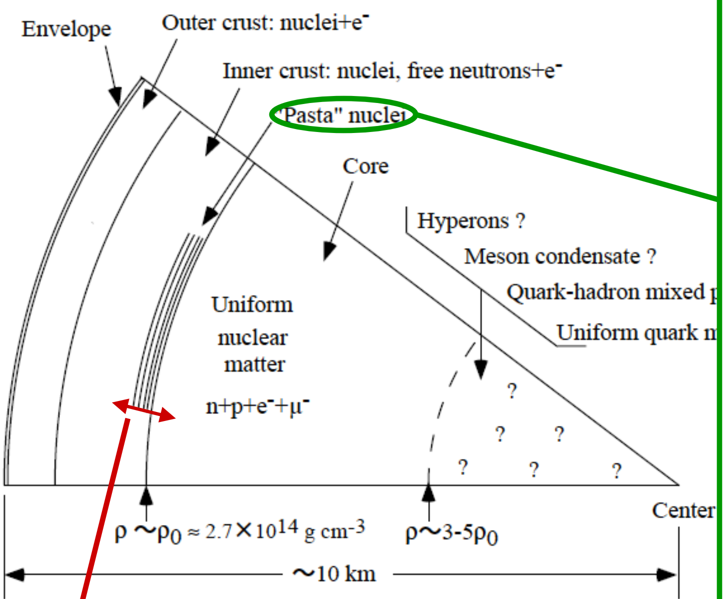

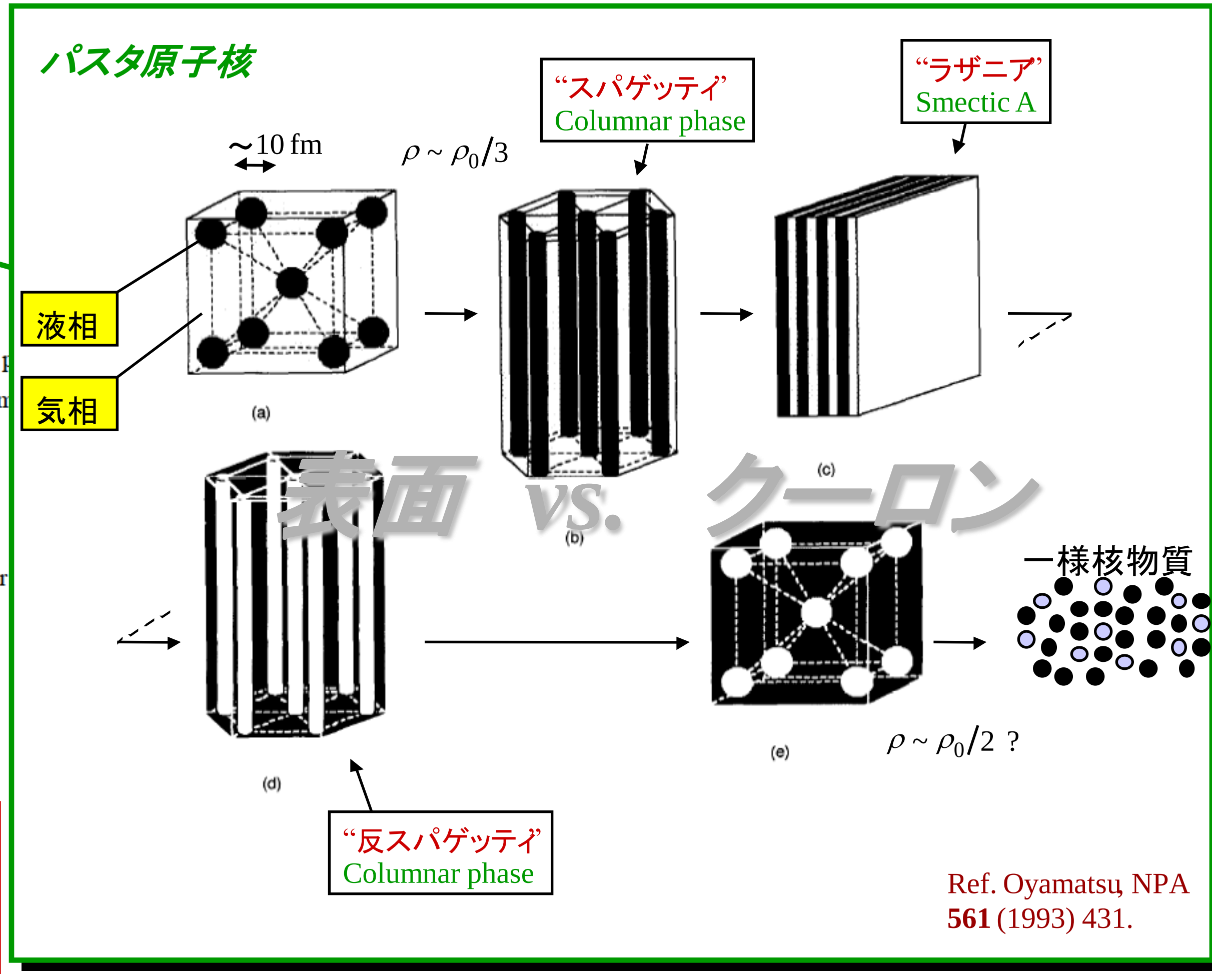

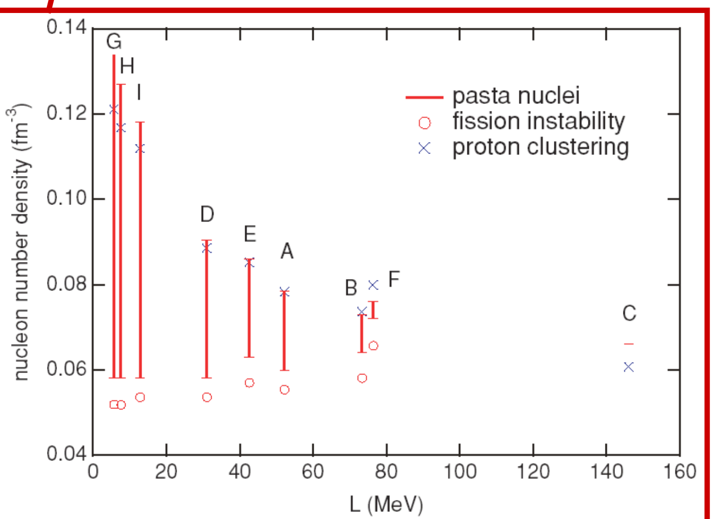

The larger *L*, the narrower pasta region.

Ref. Oyamatsu & Iida, PRC **75** (2007) 015801.

電子遮蔽と相共存 vs. 相分離

Ref. Watanabe & Iida, PRC **68** (2003) 045801.

Phase separation
(strong screening)

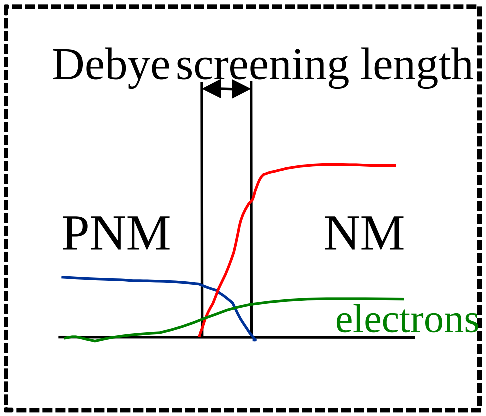

vs.

Phase mixing
(weak screening)

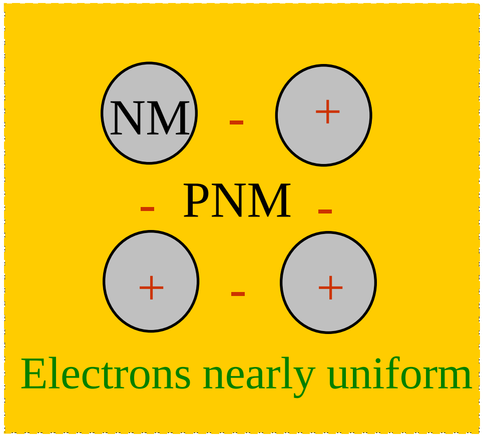

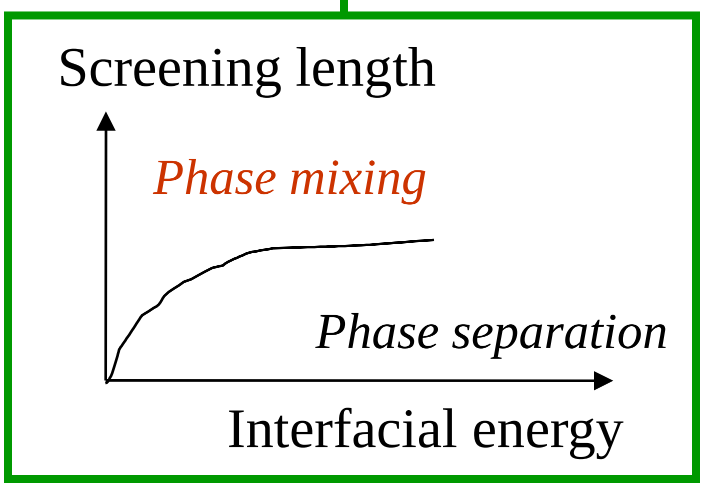

核物質の液気相転移の場合は相共存！

Pasta and symmetry energy

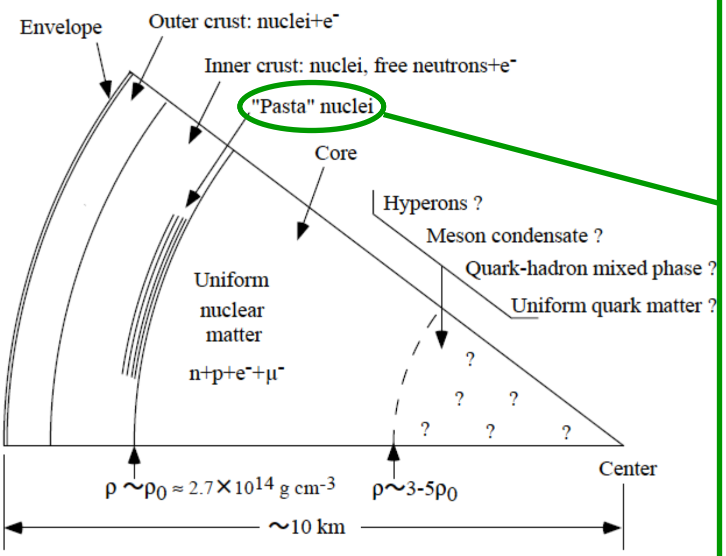

Schematic cross-section of a neutron star.

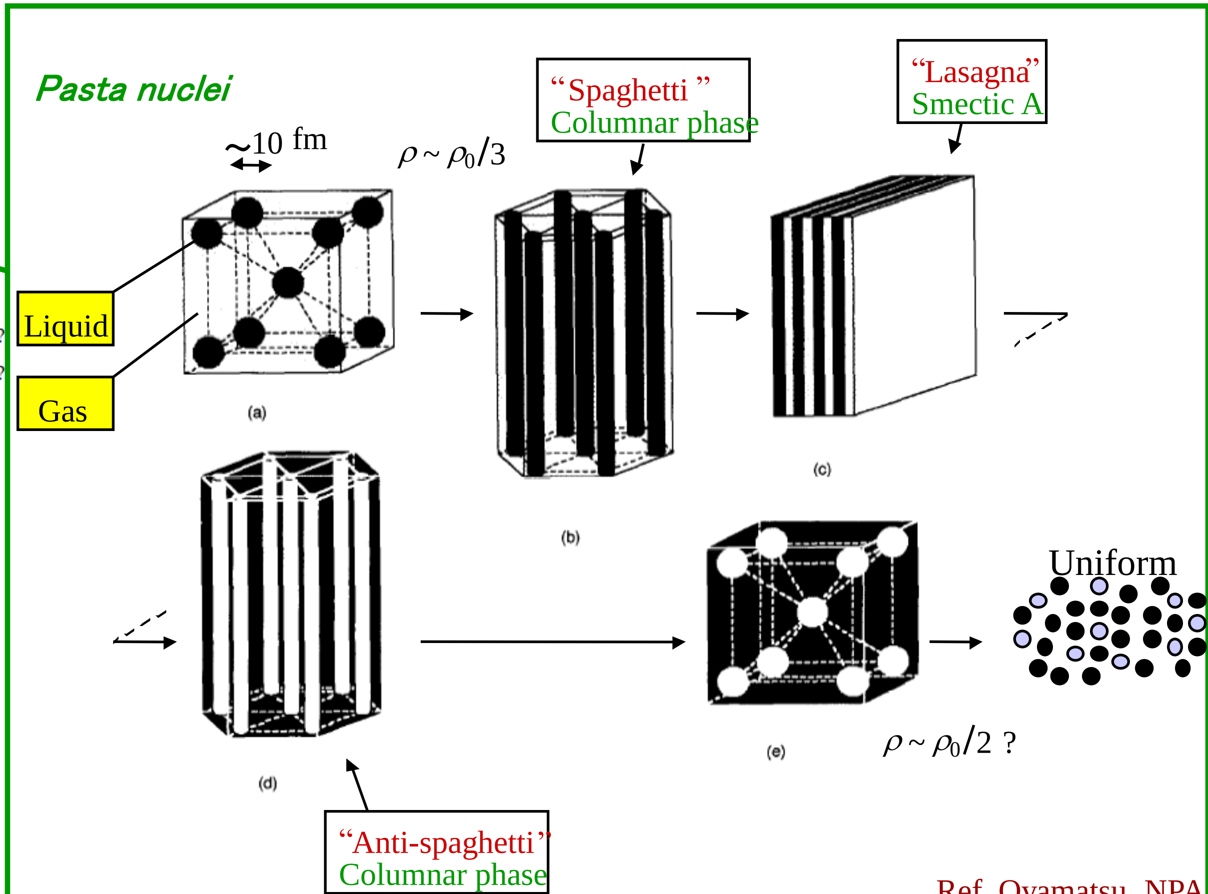

Ref. Oyamatsu, NPA **561** (1993) 431.

Symmetry energy at subnuclear densities → Proton clustering in uniform nuclear matter → Crust-core boundary

Symmetry energy at subnuclear densities → Density of dripped neutrons in the inner crust → Nuclear size

Phase diagrams from macroscopic nuclear model

Macroscopic nuclear model

For a nucleus in vacuum: Ref. Oyamatsu & Iida, PTP **109** (2003) 631.

$$-E_{\rm B}=\int d^3r\, n(\mathbf{r})w\big(n_{\rm n}(\mathbf{r}),n_{\rm p}(\mathbf{r})\big)+F_0\int d^3r\,|\nabla n(\mathbf{r})|^2+\frac{e^2}{2}\int d^3r\int d^3r'\frac{n_{\rm p}(\mathbf{r})n_{\rm p}(\mathbf{r}')}{|\mathbf{r}-\mathbf{r}'|}$$

with particle distributions (i=n,p):
$$n_i(r)=\begin{cases} n_i^{\rm in}\left[1-(r/R_i)^{t_i}\right]^3, & r<R_i\\ 0, & r\geq R_i\end{cases}$$

For a nucleus or bubble in a Wigner-Seitz cell: Ref. Oyamatsu, NPA **561** (1993) 431.

Total energy of a cell: total rest mass $-E_{\rm B}$+lattice energy+electron energy

with
$$n_i(r)=\begin{cases} \left(n_i^{\rm in}-n_i^{\rm out}\right)\left[1-(r/R_i)^{t_i}\right]^3+n_i^{\rm out}, & r<R_i\\ n_i^{\rm out}, & r\geq R_i\end{cases}$$

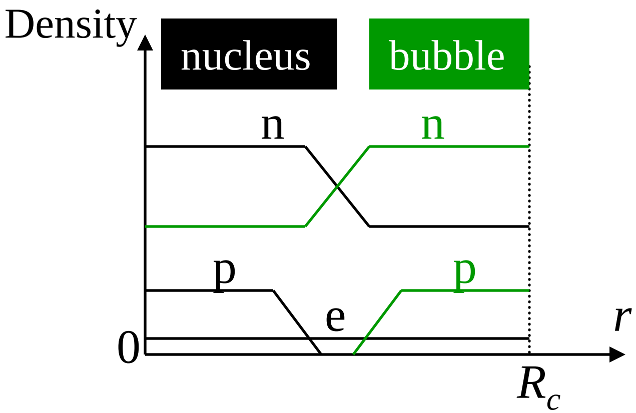

Phase diagrams from macroscopic nuclear model (contd.)

Pasta region

Ref. Oyamatsu & Iida, PRC **75** (2007) 015801.

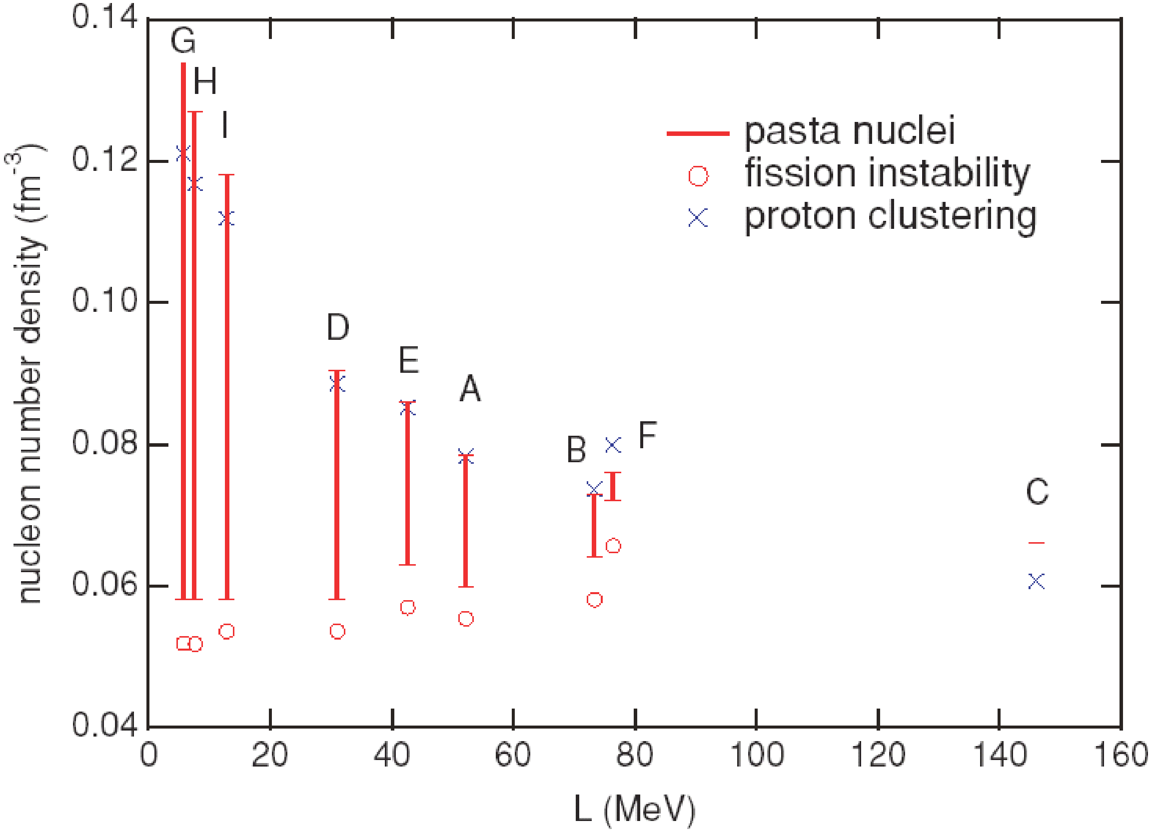

The larger *L*, the narrower pasta region.

Proton clustering and fission instability

Lower end of the pasta region

Ref. Pethick & Ravenhall, ARNPS **45** (1995) 429.

—— naïvely understood from fissionlike instability of spherical nuclei

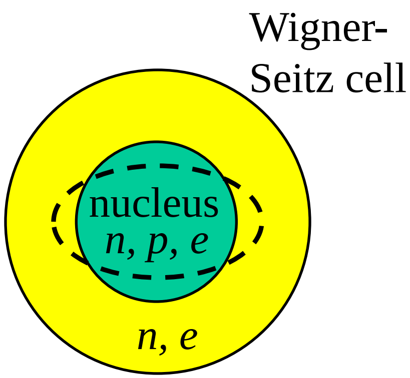

—— expected at volume fraction of about 1/8, where

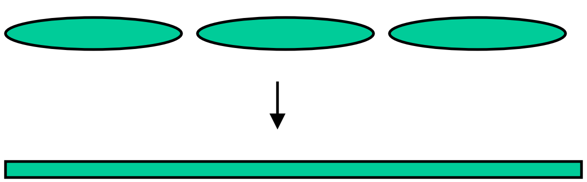

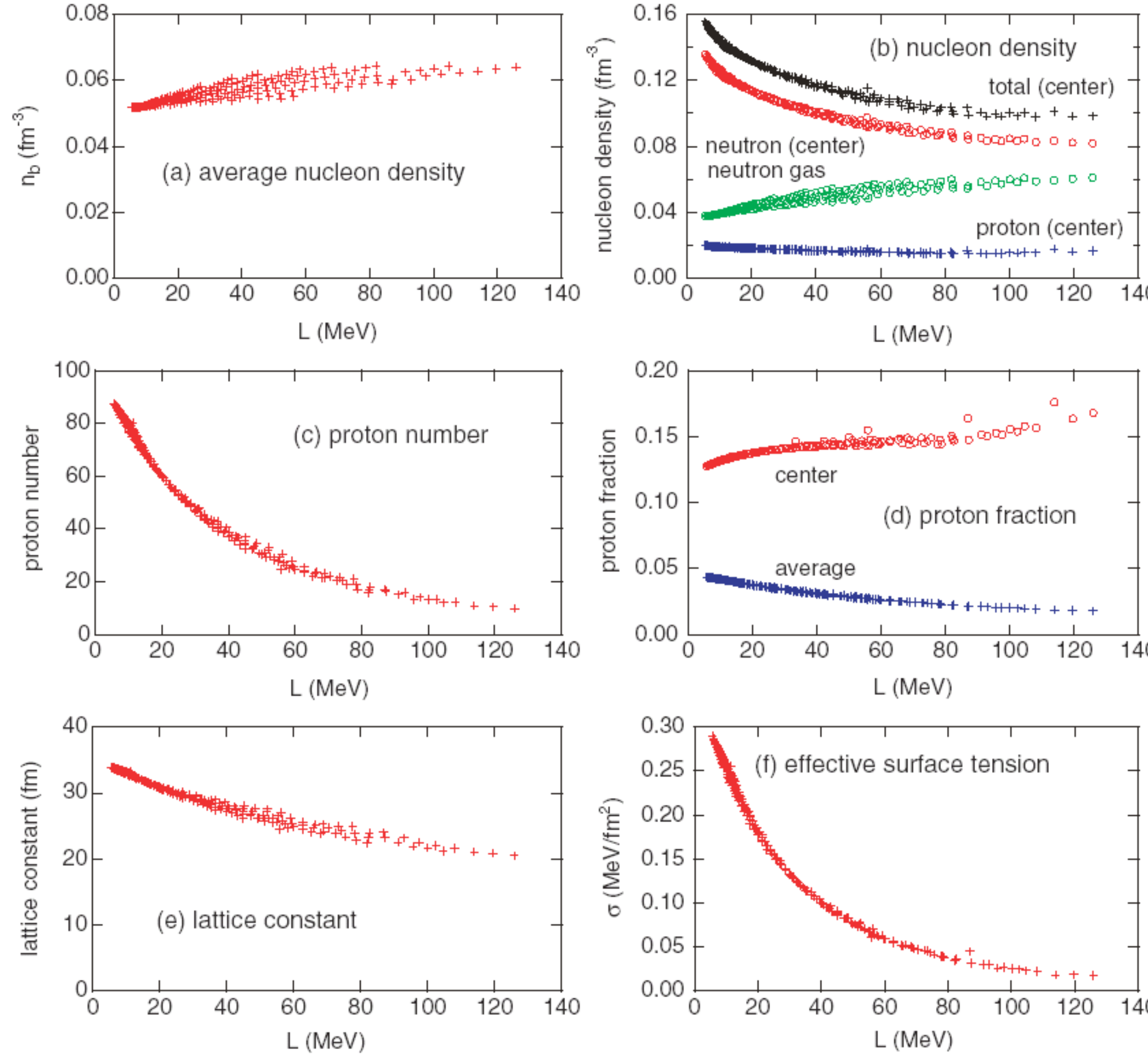

Proton clustering and fission instability (contd.)

Upper end of the pasta region

Ref. Pethick, Ravenhall, & Lorenz, NPA **584** (1995) 675.

—— naïvely understood from proton clustering instability of uniform matter

Uniform nuclear matter β equilibrated and neutralized by electrons

$$\delta n_{\mathrm{p}}(\mathbf{r})$$

$$E - E_{\mathrm{uniform}} = \frac{1}{2}\int \frac{d^3q}{(2\pi)^3} v(q) \left|\delta n_{\mathrm{p}}(\mathbf{q})\right|^2$$

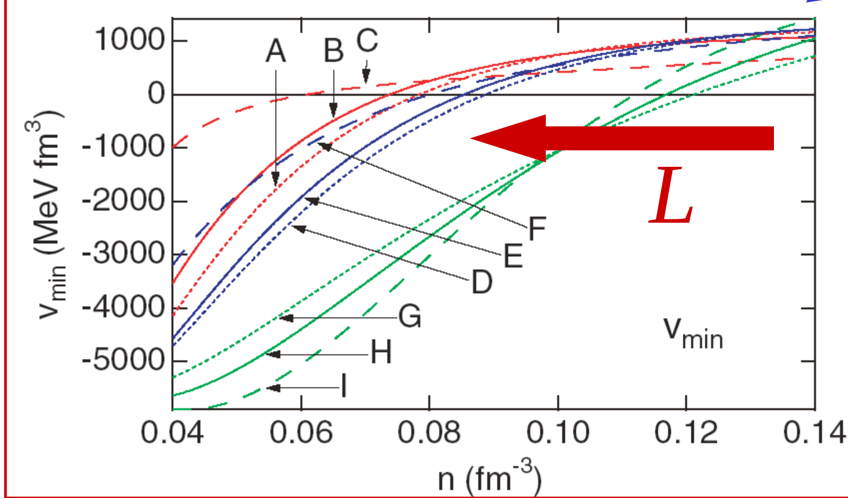

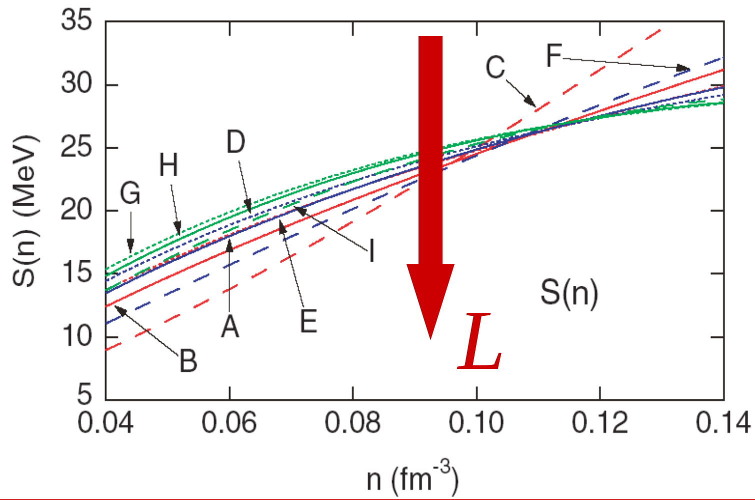

Proton clustering and fission instability (contd.)

L dependence of the onset densities

Ref. Oyamatsu & Iida, PRC **75** (2007) 015801.

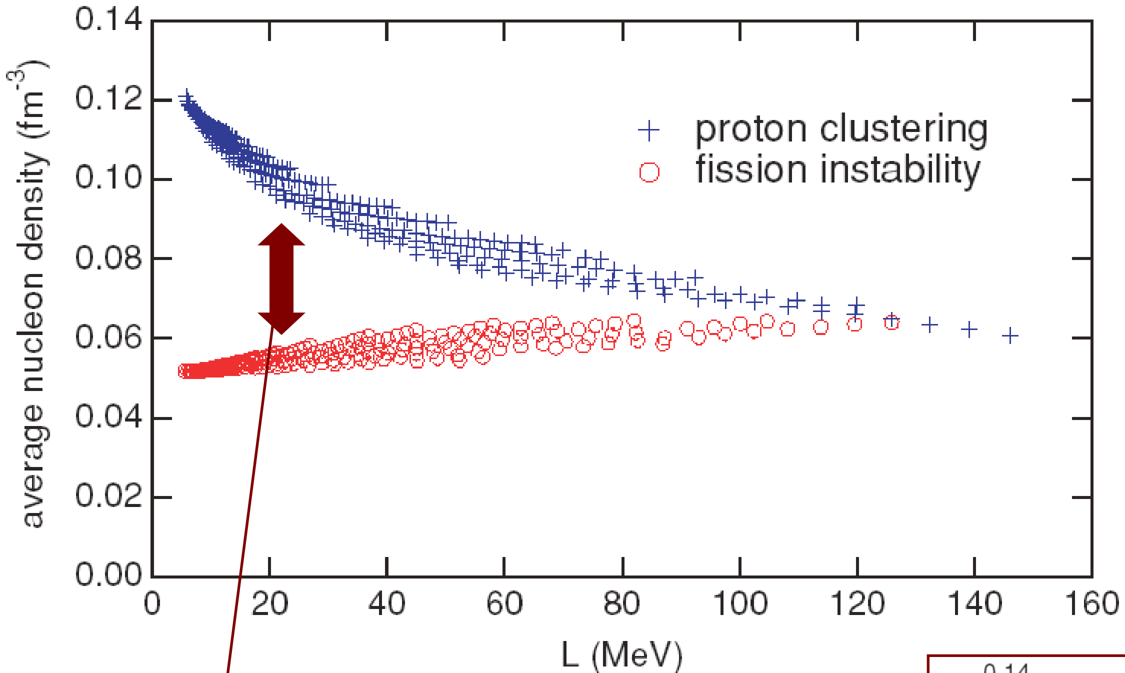

Good measure of the pasta region!

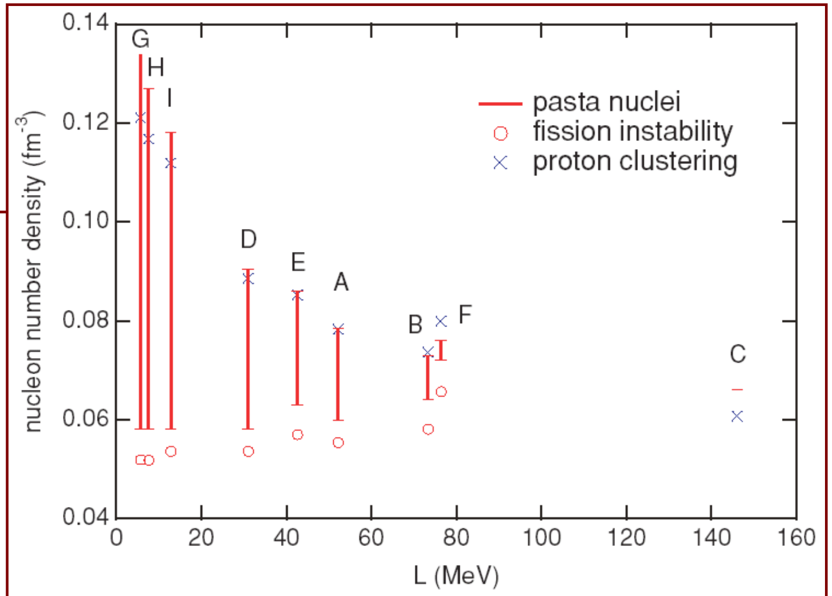

Thomas-Fermi approach to nuclear pasta beyond the Wigner-Seitz approximation

3D (grid 0.8 fm, cell size 60 fm)

Ref. Okamoto, Maruyama, Yabana, & Tatsumi, arXiv:1110.6672.

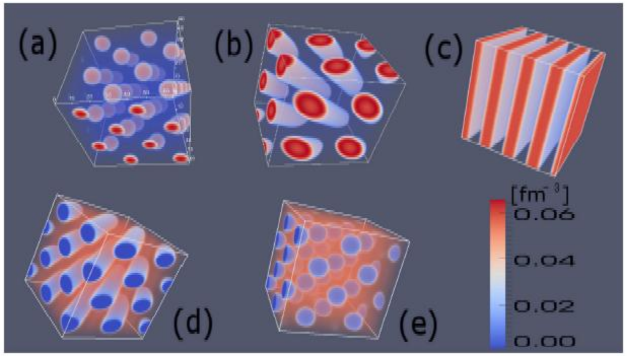

FIG. 1: (color online) Proton density distributions of the ground states of symmetric matter ($Y_p = 0.5$). Typical pasta phases are observed: (a) Spherical droplets with a fcc crystalline structure at baryon density $\rho_B = 0.01$ fm^{-3}. (b) Cylindrical rods with a honeycomb crystalline structure at 0.024 fm^{-3}. (c) Slabs at 0.05 fm^{-3}. (d) Cylindrical tubes with a honeycomb crystalline structure at 0.08 fm^{-3}. (e) Spherical bubbles with a fcc crystalline structure at 0.09 fm^{-3}.

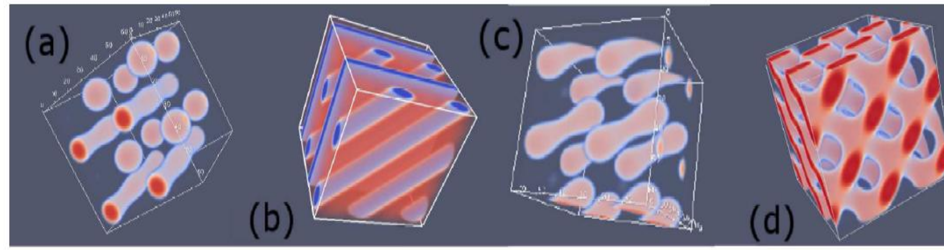

FIG. 4: Proton density distributions with complex structures ($Y_p = 0.5$). (a) mixture of droplet and rod, 0.022 fm^{-3}, (b) slab and tube, 0.068 fm^{-3} ; (c) dumbbell like structure, 0.018 fm^{-3} ; (d) diamond like structure, 0.048 fm^{-3}.

2D (grid 0.08 fm, cell size 10-20 fm)

Ref. Nakazato, Oyamatsu, & Iida, to be published.

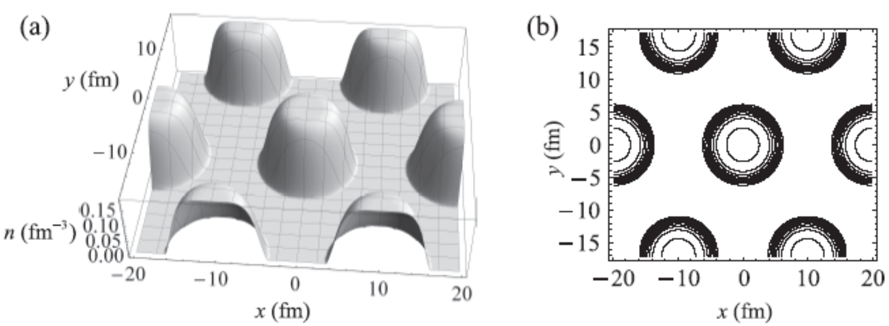

Fig. 4. Nucleon distributions for rod type nuclei with $(n_B, x_p) = (0.3n_0, 0.5)$ in (a) solid figure and in (b) contour map where the lines are drawn by steps of 0.02 fm^{-3}. The computational region is 0 fm $\leq x \leq 9.885$ fm and 0 fm $\leq y \leq \sqrt{3} \times 9.885$ fm, while the eight computational regions are connected in the depicted profiles.

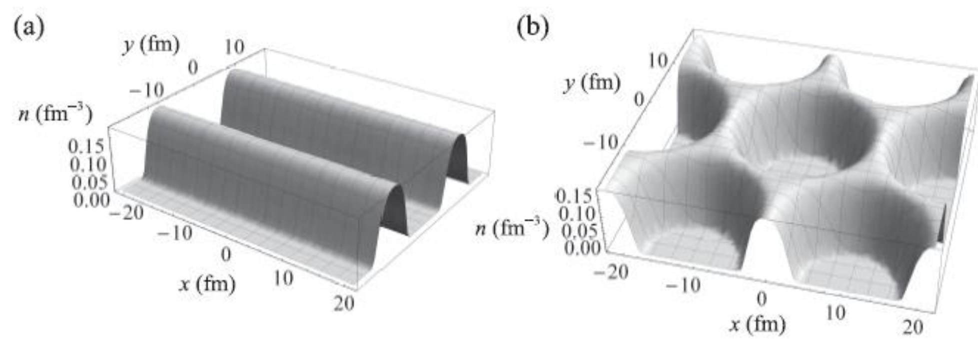

Fig. 6. Nucleon distributions for (a) slab type nuclei with $(n_B, x_p) = (0.4n_0, 0.5)$ and (b) rod-hole type nuclei with $(n_B, x_p) = (0.5n_0, 0.5)$. The eight computational regions are connected in the depicted profiles as in Fig. 4.

Gyroid

Ref. Nakazato, Iida, & Oyamatsu, arXiv:1011.3866.

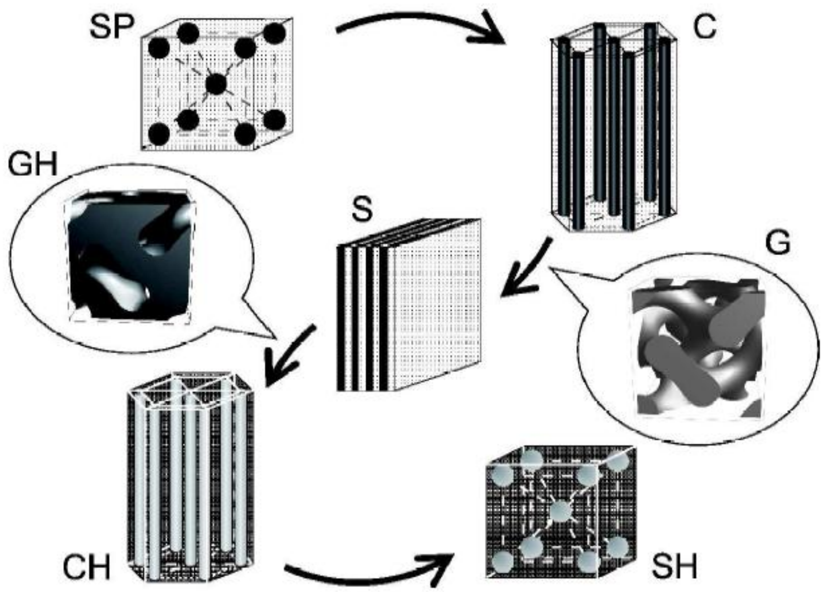

Curvature corrections (x=0.3)

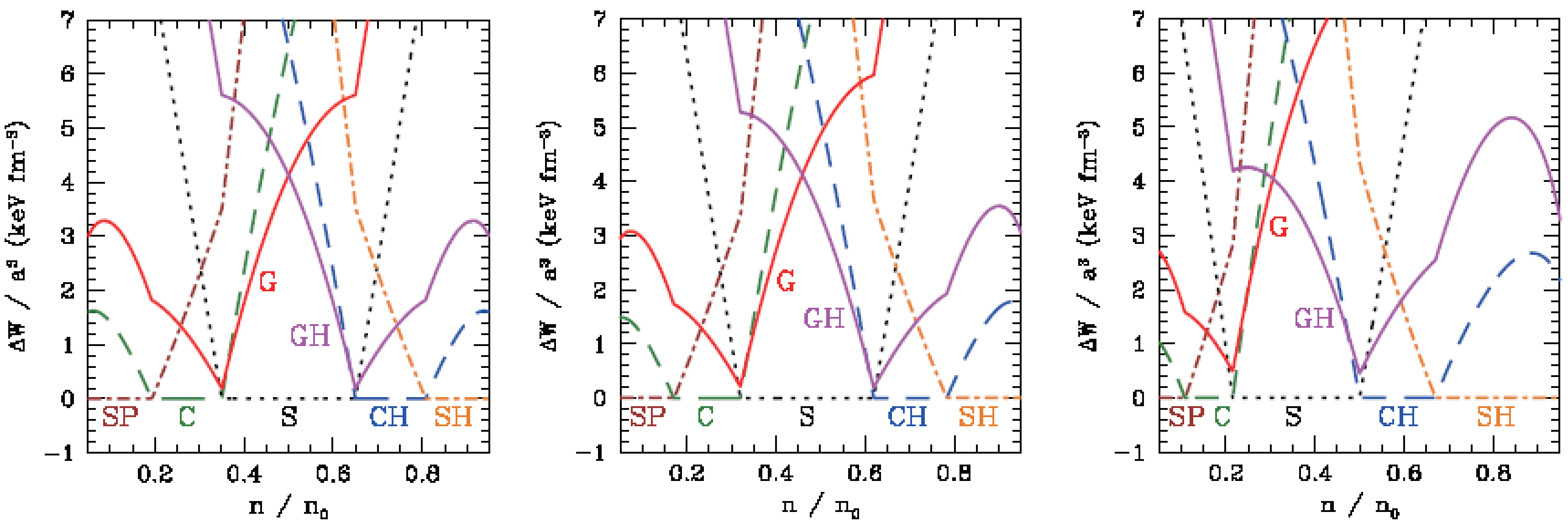

Gyroid in polymer systems

Ref. Bates & Fredrickson, Phys. Today Feb. (1999)32.

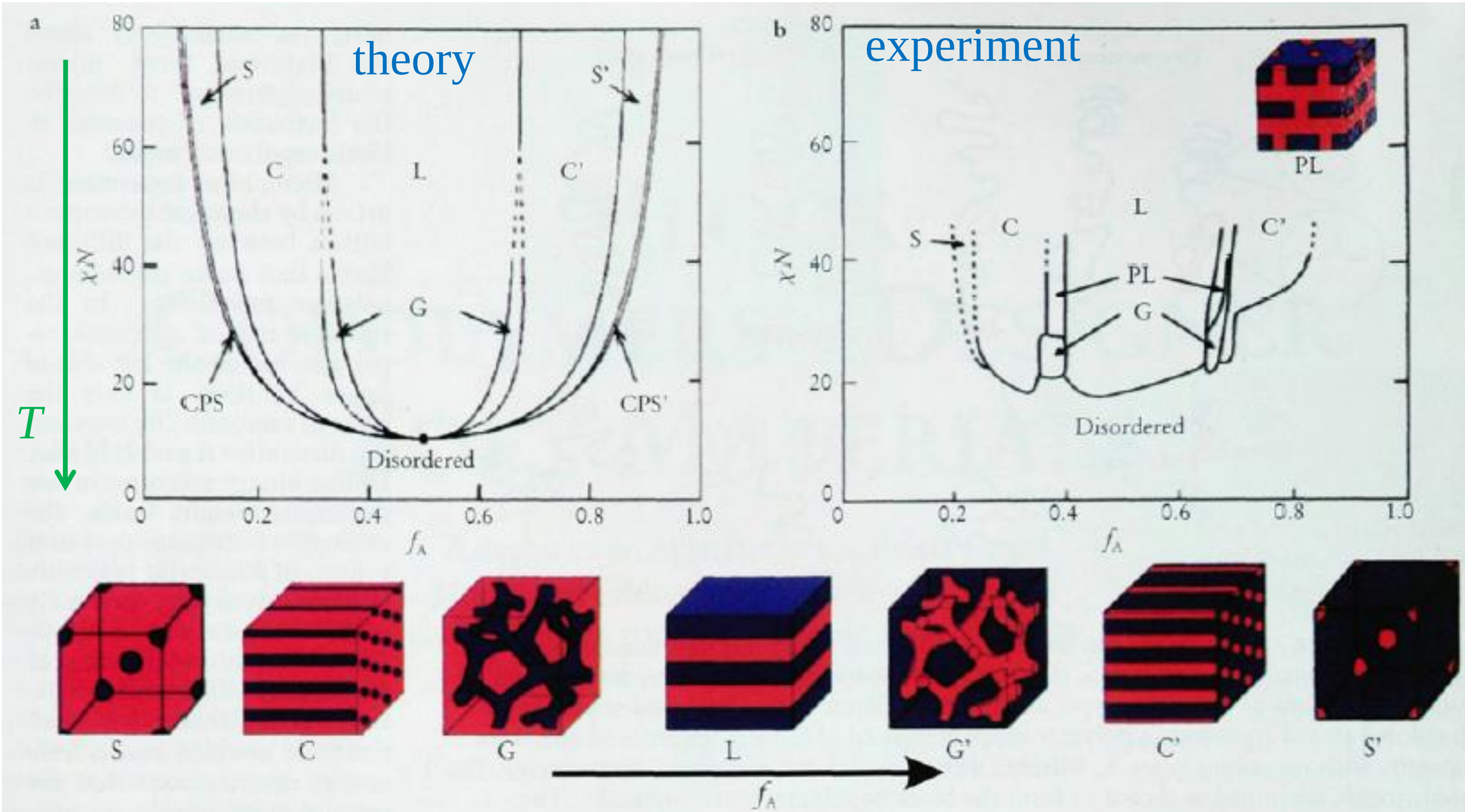

FIGURE 3. PHASE DIAGRAM for linear AB diblock copolymers, comparing theory and experiment. **a:** Self-consistent mean-field theory[8] predicts four equilibrium morphologies: spherical (S), cylindrical (C), gyroid (G) and lamellar (L), depending on the composition f and combination parameter χN. Here, χ is the segment–segment interaction energy (proportional to the heat of mixing A and B segments) and N is the degree of polymerization (number of monomers of all types per macromolecule). **b:** Experimental phase portrait for poly(isoprene-styrene) diblock copolymers.[9] The resemblance to the theoretical diagram is remarkable, though there are important differences, as discussed in the text. One difference is the observed PL phase, which is actually metastable. Shown at the bottom of the figure is a representation of the equilibrium microdomain structures as f_A is increased for fixed χN, with type A and B monomers confined to blue and red regions, respectively.

Pastas at finite temperatures

Ref. Sonoda, PhD thesis (2009, U. Tokyo).

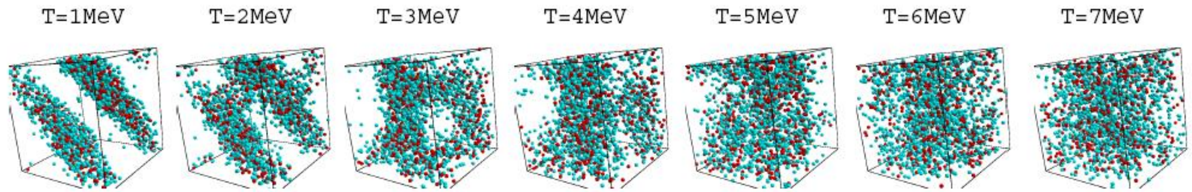

QMD model 1
(L=93 MeV)

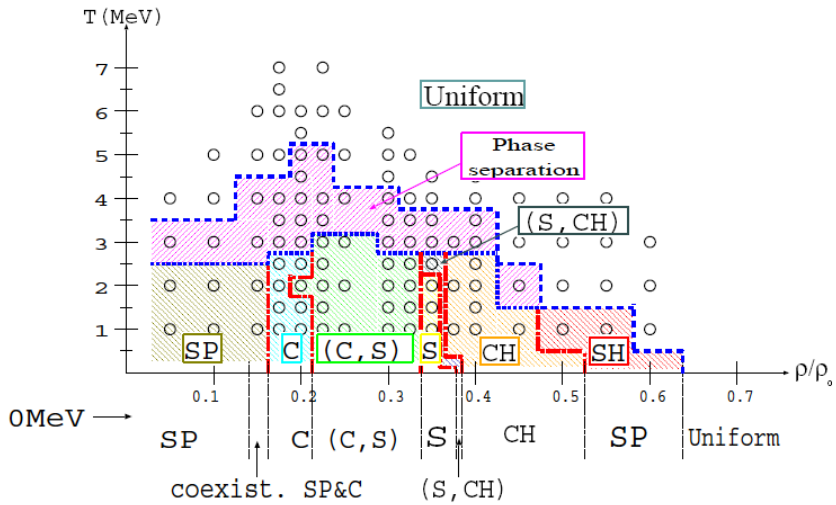

QMD model 2
(L=80 MeV)

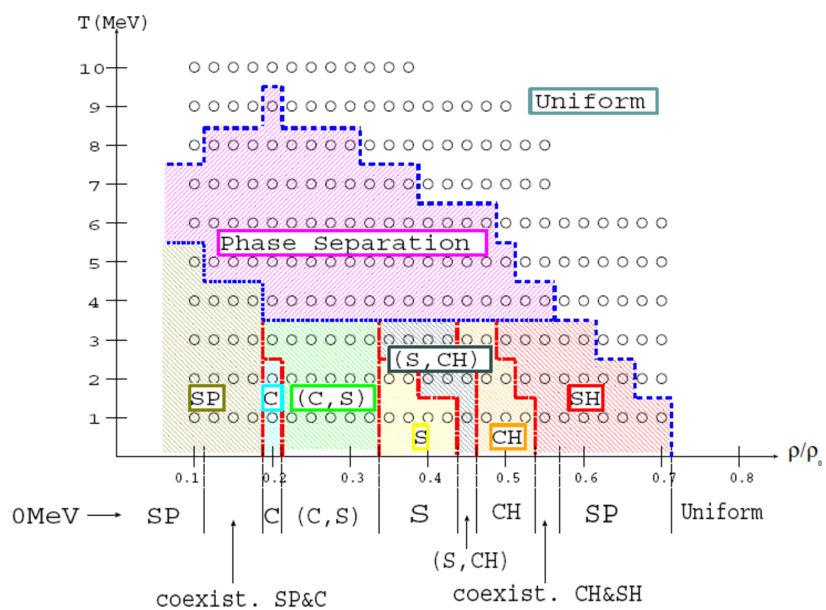

x=0.3

$T < T_c$=15–20 MeV

relevant for collapsing supernova cores

Ref. Pethick & Potekhin, PLB **427** (1998) 7.

Thermally induced fluctuations of slab and rod nuclei

Smectic A

Columnar phase

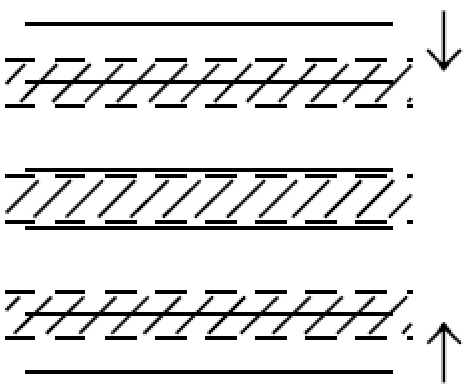

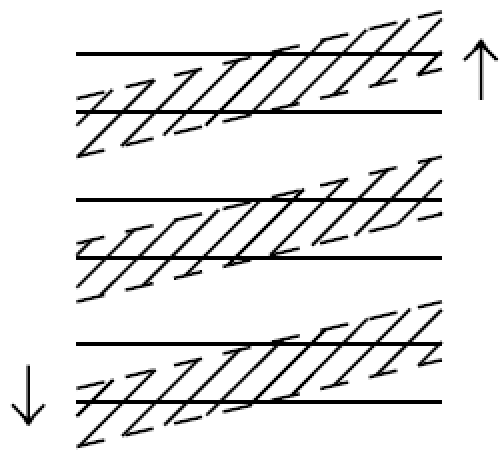

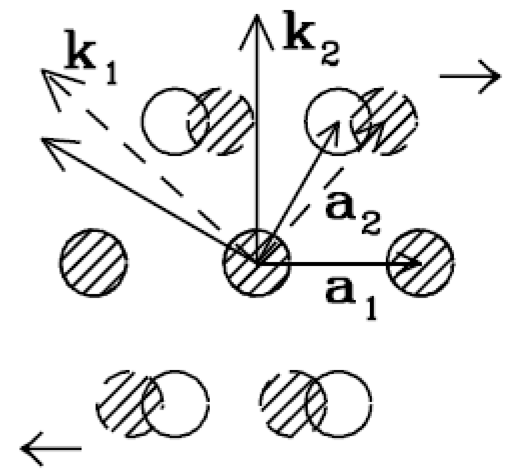

Compression

Shear

Transverse shear

Elastic properties of pasta nuclei

Change in the Coulomb and surface energies due to displacements

Pastas at finite temperatures (contd.)

Ref. Watanabe, Iida, & Sato, NPA **676** (2000) 455.

Melting temperatures determined from rms displacement vs. internuclear spacing

Smectic A

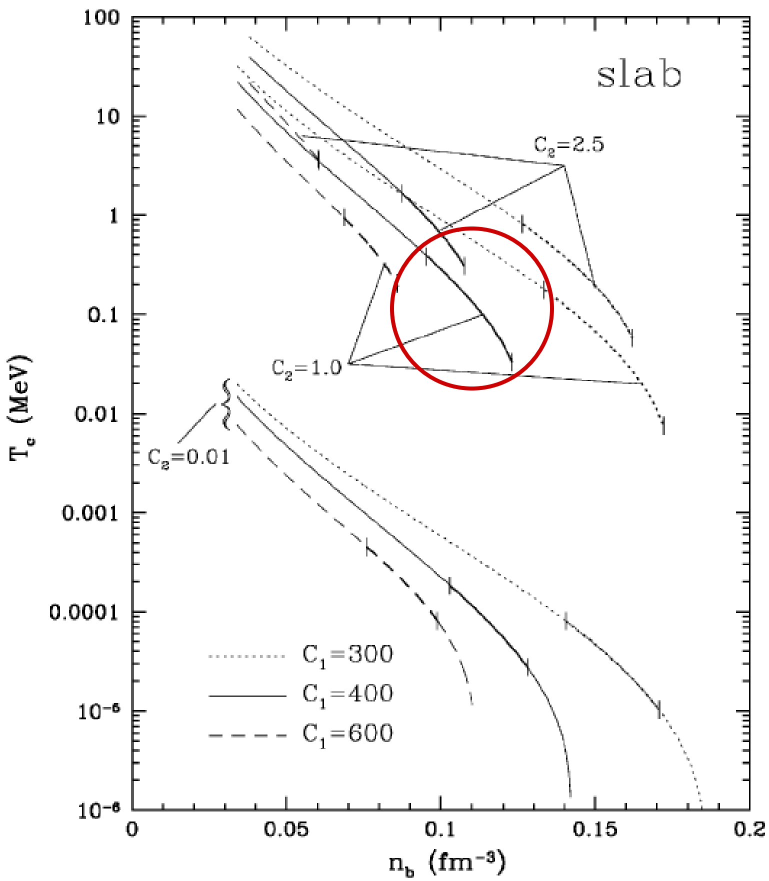

Columnar phase

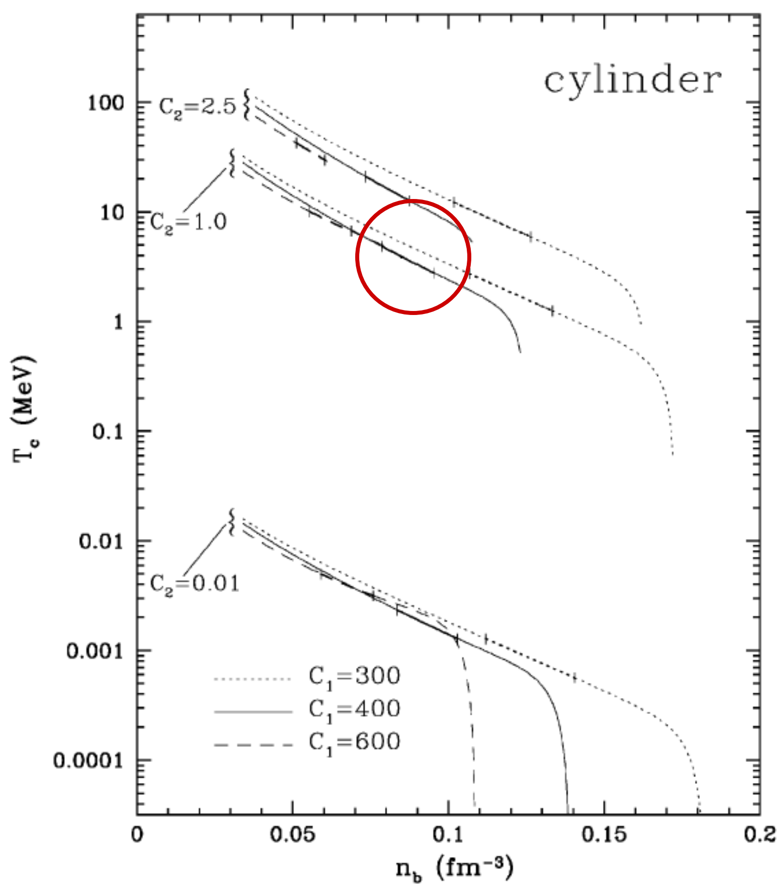

One-dimensional lattice is more susceptible to thermal fluctuations à la Landau-Peierls.

QPOs in giant flares from SGRs

マグネター

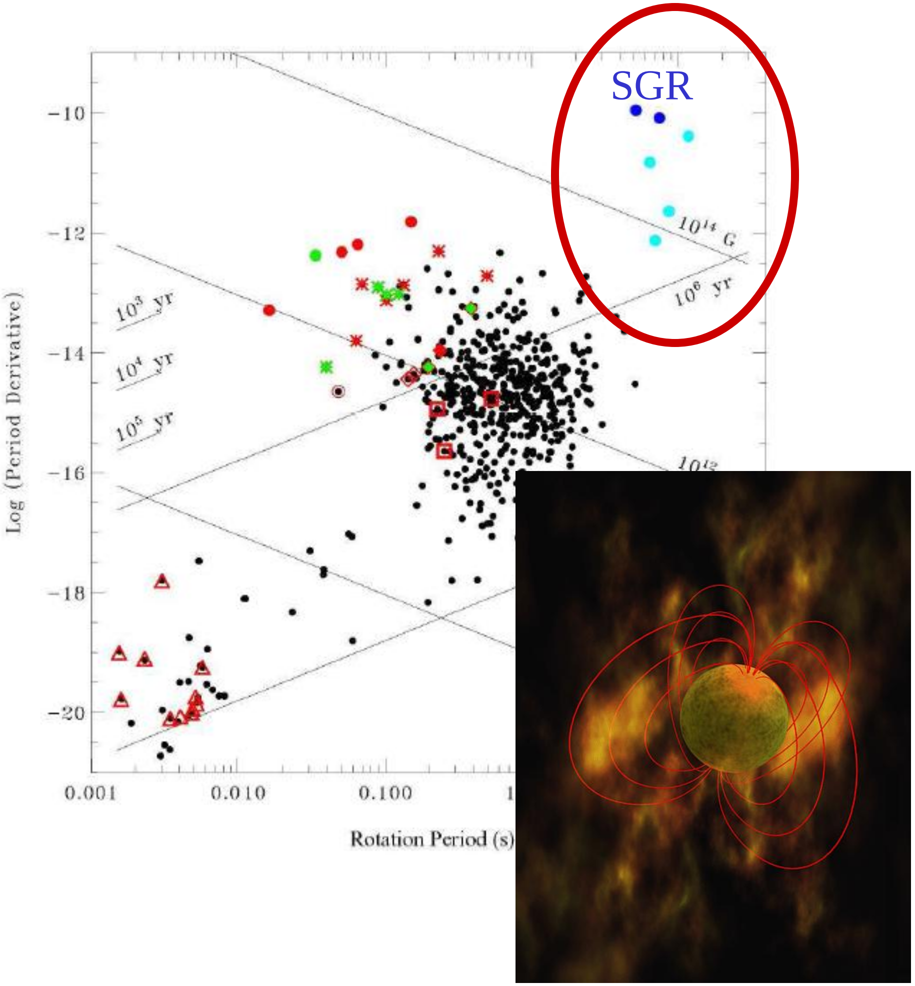

想像図
by NASA

arXiv:astro-ph/0208356

X-ray light curve of the SGR 1806-20 giant flare

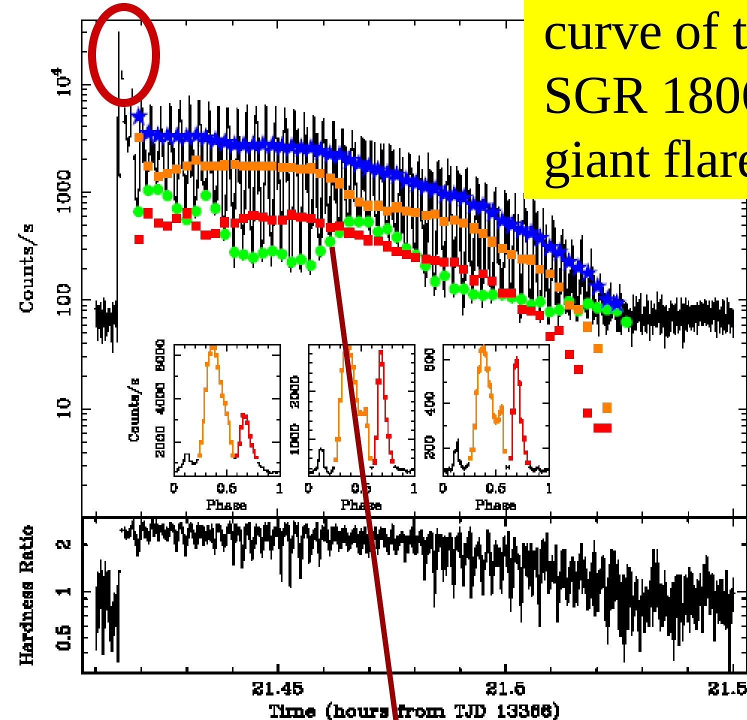

QPOs

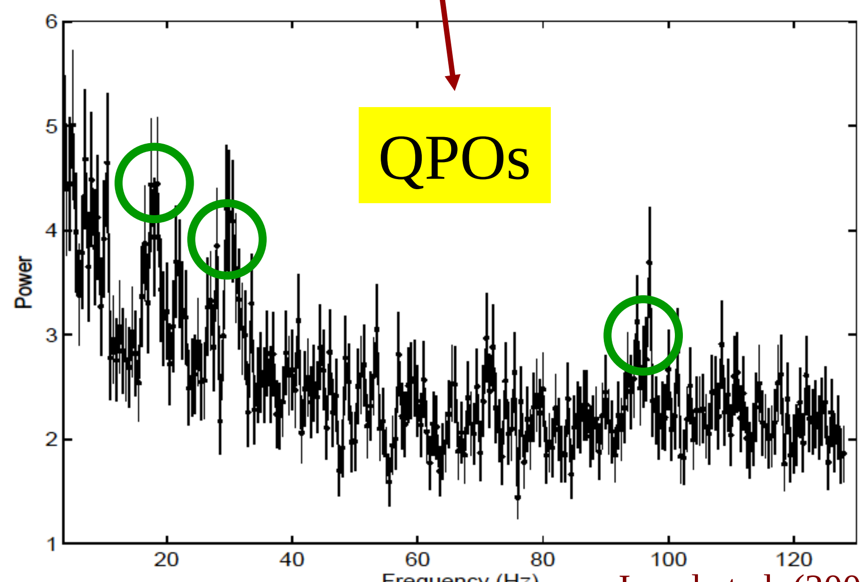

Israel et al. (2005)

QPOs in giant flares from SGRs (contd.)

同定できないものはコア
のアルベンモード？

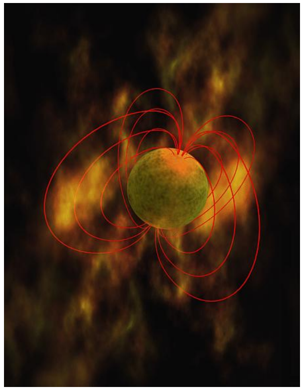

QPOをクラストのずり
モードととらえた場合
の振動数計算例

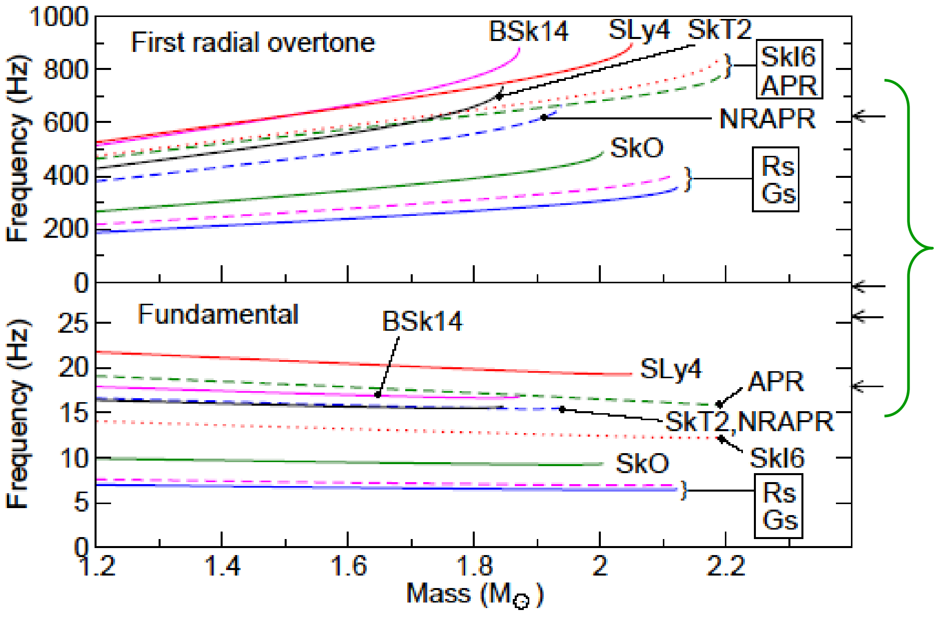

FIG. 3: The crust oscillation frequencies as a function of neutron star mass, for both the fundamental ($n = 0, l = 2$) torsional shear mode and the first radial ($n = 1$) overtone. The curves end at the maximum mass. The arrows on the right indicate QPO frequencies measured during the 2004 hyperflare from SGR 1806-20 [2, 4, 5].

Steiner & Watts (2009)

- ずり弾性率 ($\propto Z^2$) と L の関係から L に制限！？

- パスタのずり弾性率への影響は？

Equilibrium nuclear size in the inner crust of a neutron star

Ref. Oyamatsu & Iida, PRC **75** (2007) 015801.

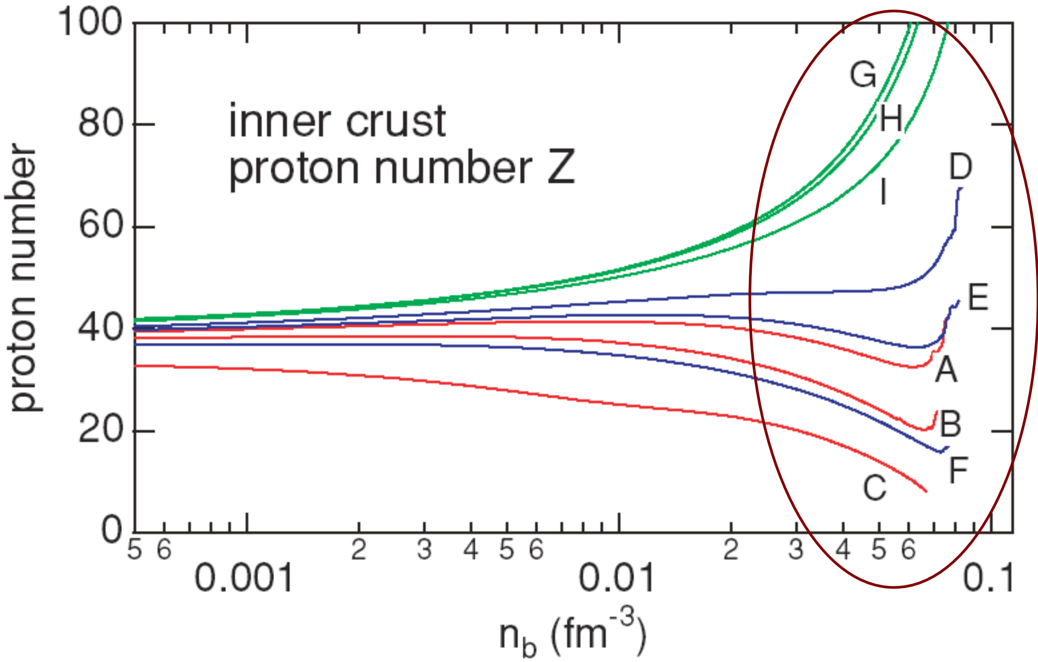

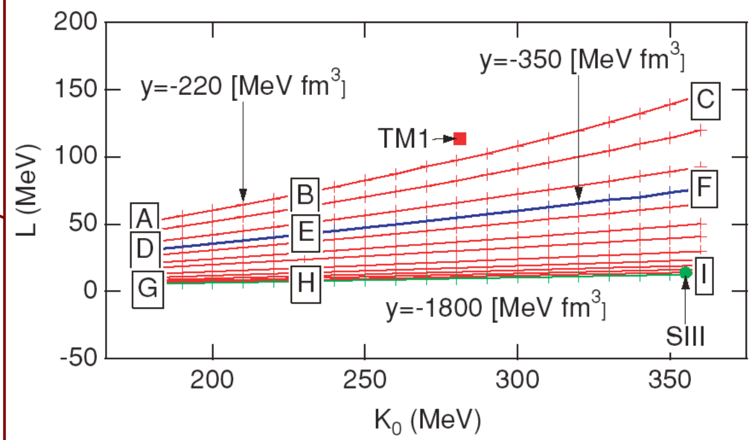

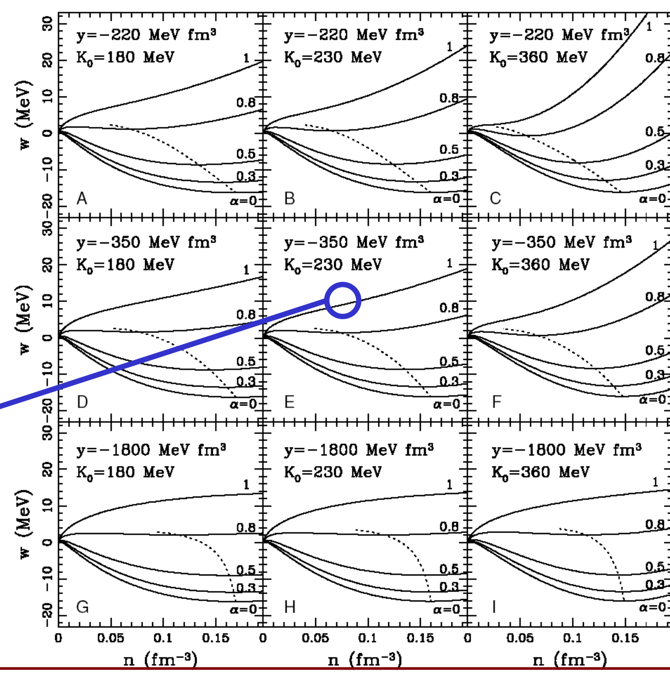

The larger *L*, the smaller size.

close to the GFMC result with the Argonne v_8' potential

Constraint on *L* from estimates of crustal torsional oscillation frequencies

Ref. Sotani, Nakazato, Iida, & Oyamatsu, arXiv:1202.6242.

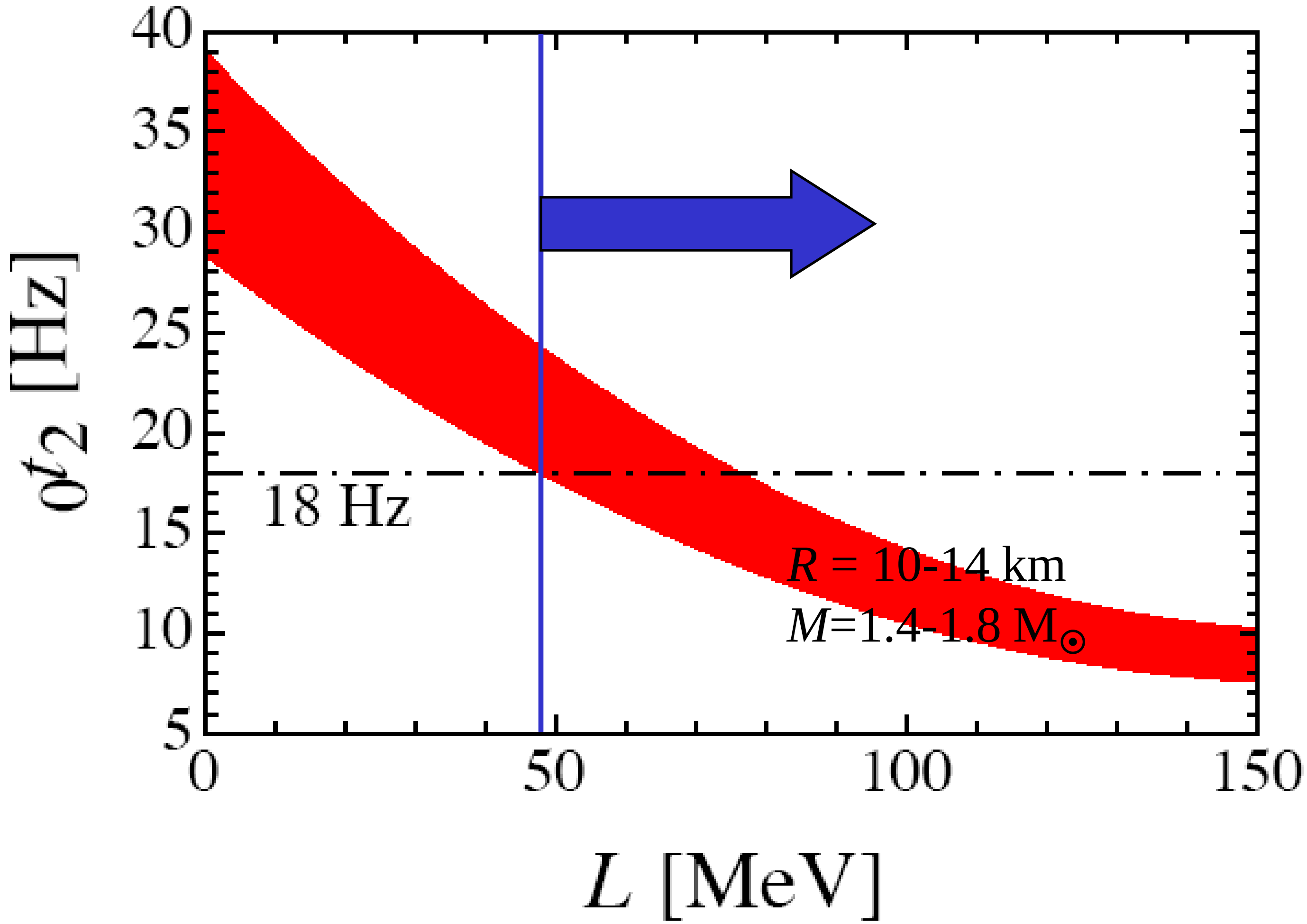

Quiescent LMXB systems

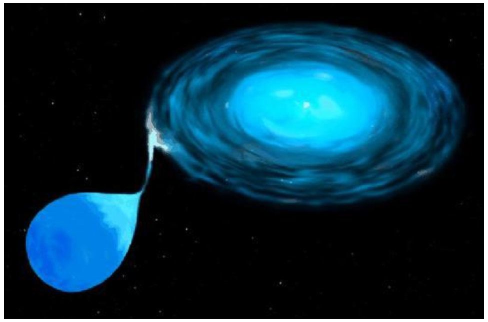

降着が止むと

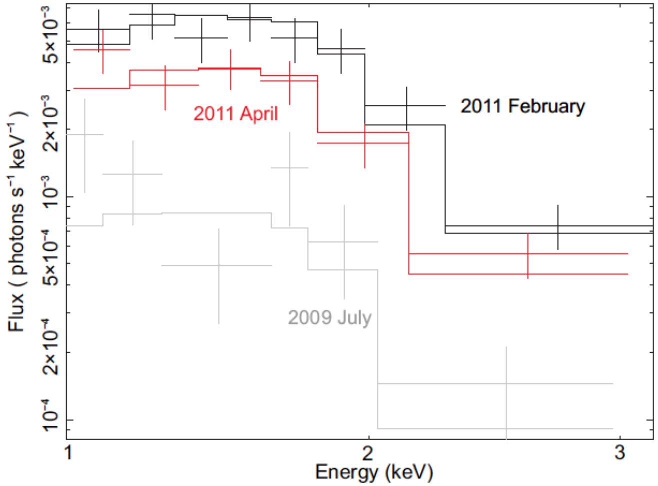

Figure 2. *Chandra*/ACIS spectra of IGR J17480–2446 at three different epochs. The 2011 data was obtained within a few months after the end of the 2010 October–December outburst and the 2009 data ~ 1 year prior to the accretion activity. The solid lines indicate best-fits to the neutron star atmosphere model NSATMOS.

Degenaar et al., arXiv:1107.5317.

Deep crustal heating during accretion

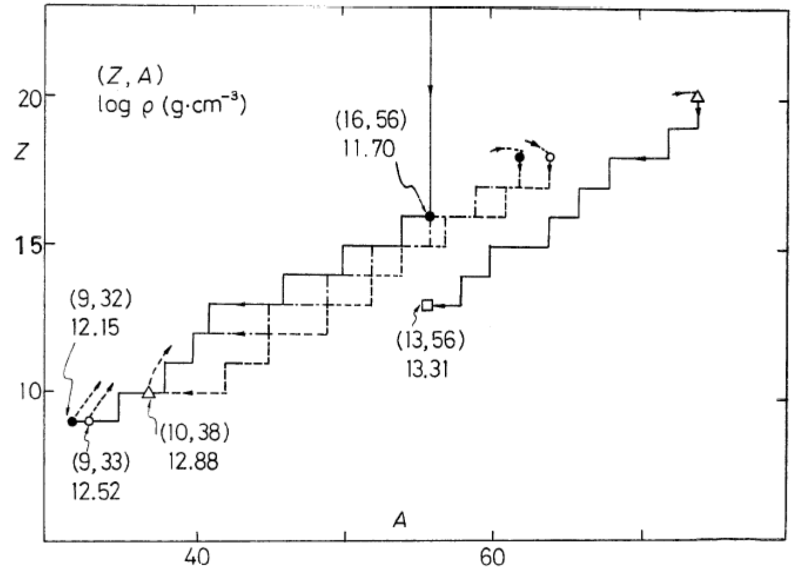

Fig. 1. Evolution of nuclear species with the increase of the density. The mark ● indicates the point of the first pycnonuclear reaction, ○ the second, △ the third and □ the fourth. The initial species is ^{56}Fe. (Model I)

K. Sato (1979)

*L*とともに反応経路はいかに変化する？

Conclusion

QPOs in giant flares from SGRs

Pasta region in neutron star crusts severely constrained

Nuclear size in neutron star crusts

$L > \sim 50$ MeV

Confirmation by Hartree-Fock calculations is desired.